Mon. Not. R. Astron. Soc. **000**, 000–000 (2000)

Non-parametric star formation histories for 5 dwarf spheroidal galaxies of the local group

X. Hernandez[1,2], Gerard Gilmore[1] and David Valls-Gabaud[3,1]
[1] *Institute of Astronomy, Cambridge University, Madingley Road, Cambridge CB3 0HA*
[2] *Instituto de Astronomía, Universidad Nacional Autónoma de México, A.P. 70-264, 04510 México, D.F.*
[3] *UMR CNRS 7550, Observatoire de Strasbourg, 11 Rue de l'Université, 67000 Strasbourg, France.*

22 February 2000

ABSTRACT

We use recent HST colour-magnitude diagrams of the resolved stellar populations of a sample of local dSph galaxies (Carina, LeoI, LeoII, Ursa Minor and Draco) to infer the star formation histories of these systems, $SFR(t)$. Applying a new variational calculus maximum likelihood method which includes a full Bayesian analysis and allows a non-parametric estimate of the function one is solving for, we infer the star formation histories of the systems studied. This method has the advantage of yielding an objective answer, as one need not assume *a priori* the form of the function one is trying to recover. The results are checked independently using Saha's W statistic. The total luminosities of the systems are used to normalize the results into physical units and derive SN type II rates. We derive the luminosity weighted mean star formation history of this sample of galaxies.

Key words: methods: statistical – stars: formation – galaxies: evolution – Local Group

1 INTRODUCTION

The local dwarf spheroidal galaxies form a sample of small galaxies which, due to their relatively nearby locations and close association with the Milky Way could in principle furnish crucial observational and theoretical information on a range of astrophysical phenomena. As these systems are eventually disrupted and incorporated into the Milky Way they illustrate locally one of the mechanisms thought to be responsible for the build up of large galaxies. Thus comparing their stars and those now found in our galaxy we can obtain a first estimate of the relevance of late mergers (Unavane et al. 1996). Dynamical studies of their stars have yielded valuable constraints on the nature and structure of dark matter halos at the smallest scales (Lin & Faber 1983, Gerhard & Spergel 1992). Their orbits probe the galactic halo in a range of distances not sampled by any other objects and can thus be used to study the outer galactic halo. Additionally, their small sizes make them in principle the simplest galactic systems, where key processes such as star formation and gas flows can be studied under relatively well defined conditions.

However, this situation is complicated by the fact that we not only lack a theoretical understanding of these systems, but also an observational record of their evolution; only a present day snapshot of their physical parameters is available, as is the case with most galactic systems. Whilst high redshift observations have recently opened up new areas of research as they begin to yield an statistical description of the evolution of bright galaxies, such an approach is likely to remain out of reach for these small systems for some time. Fortunately, their neighboring locations allow the study of their individual stars, which offers the possibility of directly probing their evolutionary histories by inferring star formation rates as a function of time, $SFR(t)'s$.

The recent availability of detailed colour-magnitude diagrams for several nearby systems has prompted the development and allowed the application of careful statistical methods aimed at reconstructing the star formation histories of these objects (e.g. Chiosi et al. (1989), Aparicio et al. (1990) and Mould et al. (1997) using Magellanic and local clusters, and Mighell & Butcher (1992), Smecker-Hane et al. (1994), Tolstoy & Saha (1996), Aparicio & Gallart (1995) and Mighell (1997) using local dSph's). Although much has been learnt of the complex $SFR(t)'s$ of these systems, existing studies have lacked two major ingredients: a homogeneous set of observations including several of the dSph galaxies does not exist, and different data sets are generally analyzed using different techniques. These two points make comparisons between the derived $SFR(t)'s$ at best risky. A further difficulty lies in the fact that the available rigorous statistical studies approach the problem paramet-

rically, which is something one should try to avoid when the actual structure of the function one is trying to recover can be crucial, as is the case when the underlying physics is unknown. An example of this last point is the case of the Carina dwarf. Hurley-Keller et al. (1998) solve for the best fitting three discrete bursts solution to the $SFR(t)$ and conclude that star formation has proceeded spasmodically, whilst Mighell (1997) uses a non parametric star count approach, albeit not a fully consistent statistical method, to obtain a more gradual solution for Carina's $SFR(t)$.

In this paper we have attempted to improve on the determination of the star formation histories of local dSph systems by addressing the two points mentioned above. We use recent HST observations of the resolved populations of a sample of dSph galaxies (Carina, LeoI, LeoII, Ursa Minor and Draco) uniformly taken and reduced, to recover the $SFR(t)$ of each, applying a new non-parametric maximum likelihood method. This allows meaningful comparisons to be made, as any systematics, at any level, will affect all our galaxies equally.

The outline of our paper is as follows: in section 2 we discuss the observations, in section 3 we include a brief outline of our method, which was introduced in our paper I (Hernandez et al. 1999). The results are presented in section 4, and in section 5 we summarize our results.

2 THE OBSERVATIONS

The main requirements of our observations were that they should comprise a homogeneous sample of local dSph galaxies, mostly in terms of the data reduction. Only such an internally consistent data set allows robust comparisons between different galaxies, once uniform data reduction and analysis methods are adopted. We extracted available archive HST data for the Carina, LeoI, LeoII, Ursa Minor and Draco galaxies, and used standard data reduction methods and standard HST calibration numbers throughout the sample (e.g. Elson et al. 1996).

The currently available data cover only small (and variable) sections of the total extent of these systems. This fact clearly limits the inferences which can be drawn to the small observed fractions, the star formation histories of these regions might not by representative of the average for a whole galaxy. While this limitation introduces an extra uncertainty to our results, it highlights the interesting possibility of studying spatial variations in the evolutionary histories of dSph galaxies, if comprehensive HST studies where undertaken. In the above sense, our results for the different galaxies refer in the strictest sense only to the fractions covered by the observed fields.

As we did not require the HR diagrams to extend much fainter than the oldest turnoff points ($M_V \approx 24-25$), or to be complete into the faintest limits (the faintest stars were in fact excluded from the analysis) the data reduction was straightforward. Our resulting CMDs do not show any systematic difference from comparable published ones for the galaxies we study. The technical details of the images used appear in the appendix.

3 THE METHOD

In this section we give a summary description of our HR diagram inversion method, which was described extensively in our paper I. In contrast with other statistical methods, we do not need to construct synthetic colour magnitude diagrams (CMD) for each of the possible star formation histories being considered. Rather we use a direct approach which solves for the best $SFR(t)$ compatible with the stellar evolutionary models assumed and the observations used.

The evolutionary model consists of an isochrone library, and an IMF. Our results are largely insensitive to the details of the latter, for which we use:

$$\rho(m) \propto \begin{cases} m^{-1.3} & 0.08M_\odot < m \leq 0.5M_\odot \\ m^{-2.2} & 0.5M_\odot < m \leq 1.0M_\odot \\ m^{-2.7} & 1.0M_\odot < m \end{cases} \quad (1)$$

The above fit was derived by Kroupa et al. (1993) for a large sample towards both galactic poles and all the solar neighborhood.

As the weak metallicity dispersions measured in the galaxies we are studying (around 0.3 dex) are comparable to the errors in the metallicity determinations themselves, we have not attempted to introduce any enrichment histories for any of our galaxies. In fact, as small internal metallicity spreads present in these galaxies would introduce only small differential age offsets in our inferred $SFR(t)$ (see Table I), we shall in all cases use single metallicity isochrone sets. Once a metallicity has been selected, we use the latest Padova isochrones (Fagotto et al. 1994, Girardi et al. 1996) together with a detailed constant phase interpolation scheme using only stars at constant evolutionary phase, to construct an isochrone library having a chosen temporal resolution.

In this case we implement the method with a resolution of 0.15 Gyr, sufficient for our present problem. It is one of the advantages of the method that this resolution can be increased arbitrarily (up to the stellar model resolution) with computation times scaling only linearly with it.

Our only other inputs are the positions of, say n observed stars in the HR diagram, each having a colour and luminosity, c_i and l_i. Starting from a full likelihood model, we first construct the probability that the n observed stars resulted from a certain $SFR(t)$. This will be given by:

$$\mathcal{L} = \prod_{i=1}^{n} \left(\int_{t_0}^{t_1} SFR(t) G_i(t) dt \right), \quad (2)$$

where

$$G_i(t) = \frac{\rho(l_i;t)}{\sqrt{2\pi}\sigma(l_i)} exp\left(\frac{-[C(l_i;t)-c_i]^2}{2\sigma^2(l_i)} \right)$$

In the above expression $\rho(l_i;t)$ is the density of points along the isochrone of age t, around the luminosity of star i, and is determined by the assumed IMF together with the duration of the differential phase around the luminosity of star i. t_0 and t_1 are a maximum and a minimum time needed to be considered, for example 0 and 15 Gyr. $\sigma(l_i)$ is the amplitude of the observational errors in the colour of the stars, which are a function of the luminosity of the stars. This function is supplied by the particular observational sample one is analyzing. Finally, $C(l_i;t)$ is the colour the observed star would actually have if it had formed at time t. We shall

refer to $G_i(t)$ as the likelihood matrix, since each element represents the probability that a given star, i, was actually formed at time t. Since the colour of a star having a given luminosity and age can sometimes be multi-valued function, in practice we check along a given isochrone, to find all possible masses a given observed star might have as a function of time, and add all contributions (mostly 1, sometimes 2 and occasionally 3) in the same $G_i(t)$. In this construction we are only considering observational errors in the colour, and not in the luminosity of the stars. The generalization to a two dimensional error ellipsoid is trivial, however the observational errors in colour dominate the problem to the extent of making this refinement unnecessary. Although the amplitude of luminosity errors is only a factor of ≈ 2 smaller than colour errors, as can be inferred from the fact that CMD diagrams typically display a range of luminosities 5 times larger than in colour, in discriminating between isochrones, errors in colour are $\approx$ 10 times as important as errors in luminosity. The absence of a colour dependence from $\rho(l_i;t)$ is a direct consequence of having neglected errors in the luminosity of the stars. A star of a given observed luminosity and assumed age will thus have a colour determined by the isochrones used.

Equation (2) is essentially the extension from the case of a discrete $SFR(t)$ used by Tolstoy & Saha (1996), to the case of a continuous function (continuous in time, but obviously discrete with respect to the stars) in the construction of the likelihood. The challenge now is to find the optimum $SFR(t)$ without evaluating equation (2) i.e. without introducing a fixed set of test $SFR(t)$ cases from which one is selected.

The condition that $\mathcal{L}(SFR)$ has an extremal can be written as

$$\delta\mathcal{L}(SFR) = 0,$$

and a variational calculus treatment of the problem applied. Firstly, we develop the product over i using the chain rule for the variational derivative, and divide the resulting sum by $\mathcal{L}$ to obtain:

$$\sum_{i=1}^{n}\left(\frac{\delta\int_{t_0}^{t_1} SFR(t)G_i(t)dt}{\int_{t_0}^{t_1} SFR(t)G_i(t)dt}\right) = 0 \qquad (3)$$

Introducing the new variable $Y(t)$ defined as:

$$Y(t) = \int\sqrt{SFR(t)}dt \Longrightarrow SFR(t) = \left(\frac{dY(t)}{dt}\right)^2$$

and introducing the above expression into equation (3) we can develop the Euler equation to yield,

$$\frac{d^2Y(t)}{dt^2}\sum_{i=1}^{n}\left(\frac{G_i(t)}{I(i)}\right) = -\frac{dY(t)}{dt}\sum_{i=1}^{n}\left(\frac{dG_i/dt}{I(i)}\right) \qquad (4)$$

where

$$I(i) = \int_{t_0}^{t_1} SFR(t)G_i(t)dt$$

This in effect has transformed the problem from one of searching for a function which maximizes a product of integrals (equation 2) to one of solving an integro-differential equation (equation 4). We solve this equation iteratively, with the boundary condition SFR(15)=0. Details of the numerical procedure required to ensure convergence to the maximum likelihood SFR(t) can be found in our paper I, where the method is tested extensively using synthetic HR diagrams. The main advantages of our method over other maximum likelihood schemes are the totally non parametric approach the variational calculus treatment allows, and the efficient computational procedure, where no time consuming repeated comparisons between synthetic and observational CMD are necessary, as the optimal $SFR(t)$ is solved for directly.

Table 1. Age offset in Gyr between simulated and recovered populations as a function of input age (in Gyr) and metallicity (in solar units), for a ± 0.2 dex metallicity mismatch

$[Fe/H]$	-1.4	-1.6	-1.8	-2.0	-2.2
2 Gyr	+0.6	+0.4 -0.3	+0.3 -0.1	+0.4 -0.2	-0.2
4 Gyr	+0.8	+0.5 -0.6	+0.4 -0.4	+0.6 -0.2	-0.4
6 Gyr	+1.6	+0.5 -0.9	+0.7 -0.2	+0.9 -0.5	-0.6
8 Gyr	+1.8	+0.4 -1.3	+0.5 -0.8	+1.4 -0.6	-0.9
10 Gyr	+2.5	+0.5 -2.0	+0.7 -0.5	+1.3 -0.7	-1.5

The lower main sequence region of the CMD diagram is totally degenerate with age, and contains the lower brightness stars, where the errors are larger. We have seen from using synthetic HR diagrams that excluding this region produces a faster and more accurate convergence of the method, and have in analyzing real galaxies excluded stars of magnitudes fainter than $M_V \approx +5$. This last cut together with the fact that our isochrones only extend out to the tip of the red giant branch (to go further would necessitate combining results from different physical models, which we preferred not to do) leaves us with a mass range which actually varies as a function of time. To include also the fraction of the $SFR(t)$ outside this region, we apply a minor correction factor to the result of equation (4), which accounts for the fraction of mass outside the sampled range, as a function of time, as given by the IMF used.

Before presenting the star formation histories which result from applying our method to the colour-magnitude diagrams of the galaxies sampled, we include a summary of the systematic errors associated with the theoretical inputs of the method, which are more extensively discussed in our paper I.

The IMF convolved with the duration of the differential evolutionary phase enters the calculation of the likelihood matrix in determining the density of points around the luminosity of each observed star, for each of the isochrones considered. As the main sequence and the giant branch regions of the CMD are degenerate with age (for a single metallicity population), it is the region containing the turn-off points of the sampled population that drives the solution of the

problem. As a consequence of the above, the details of the IMF used are largely unimportant, it is basically the main sequence lifetime of a star that the solution is sensitive to. This was shown explicitly in our paper I through the use of synthetic HR diagrams, where the IMF affected only the amplitude of the recovered $SFR(t)'s$, which were normalized through the total number of stars in the HR diagrams. As in this case we are normalizing the inferred $SFR(t)'s$ through the total luminosities of the galaxies being studied, changing the IMF within any reasonable limits leaves the results unaffected. The effect of any blended binaries is equally unimportant, as the broadening of the main sequence occurs in the degenerate region and is in any case much smaller than the broadening produced by the observational colour spread.

The resolution of the method varies as a function of time and of the observational errors present in the CMD being analyzed, in ways that were studied in our paper I. The observational errors tend to smear the time structure in the $SFR(t)$ always towards older ages, i.e. a burst of age t will be recovered as an episode of duration Δt ending at time t. This Δt varies with age, becoming significant ($> 1Gyr$) only for populations older than around 10 Gyr, for the level of observational errors present in our HST colour-magnitude diagrams. Younger populations are less affected, and the formal resolution at which the method was implemented of 0.15 Gyr is representative of our results for ages younger than 6 Gyr.

As explained in the previous section, our isochrones end at the tip of the red giant branch, which means that more advanced evolutionary phases can not be incorporated into the analysis. Fortunately, these later phases occupy regions of the CMD diagram distinct from those containing the phases we account for. Therefore, we can simply remove any red clump and horizontal branch stars from the analysis, leaving the structure of the studied regions unaffected. These later phases form only a minority component, containing little extra information, and do not affect our inferences. In the same way our results are not affected by the presence of some contaminating field stars. Provided they do not fall on the region of the CMD containing the turn off points of the underlying stars, they are simply removed from the analysis.

We are however sensitive to the assumed metallicity of the stellar populations being treated. In our paper I we presented a few examples of how the method reacts when inverting a synthetic HR diagram produced with isochrones different to the ones used in the inference procedure. If we construct the likelihood matrix using isochrones which are very different (about 1 dex) from the ones used to produce the HR diagram, the iterative method used in solving equation (4) becomes unstable and tends to divergent solutions. This property can be used to deduce large incompatibilities between the stars and the template isochrones against which they are being compared. Small metallicity offsets are much harder to detect, and produce distorted results. The degree of distortion varies with age, shape of the overall $SFR(t)$ and the observational errors present in highly non-linear fashion.

To give some indication of these distortions we present Table I. We produced a synthetic HR diagram from a single Gaussian burst input $SFR(t)$ having a duration of 1 Gyr, of a given metallicity, and applied the method using a metallicity 0.2 dex lower than the one used to generate the stars. This was repeated for a range of metallicities and ages, for both positive and negative metallicity mismatches. The top row of Table 1 shows the input metallicity (in dex), the first column shows the input burst age, and the other entries show the age offset between the recovered and input $SFR(t)$, all ages are given in Gyr. A "+" sign denotes the inferred population was older than the input one, where a lower metallicity was used in the inference procedure. Similarly, a "-" indicates that the inferred population was younger than the input one, where a higher metallicity was used to invert the simulated CMD.

The metallicities shown cover the range present in the galaxies being studied. Populations much younger than 2 Gyr are not present in our galaxies, and those older than 10 Gyr are distorted by the observational errors to the point of eliminating much of the time resolution of the inversion in this region. This table can be used to estimate the effects of changing the assumed metallicities, or of introducing temporal gradients, within the small observationally restricted range. The well known age-metallicity degeneracy is apparent. This might affect our results even if the mean metallicity is well known, as temporal variations in the metallicities (which must exist at some level) are not considered by the method. Using an independent test on our results, we find these effects to be minor in most of the cases we study, as observational measurements of the metallicity of these systems suggest.

3.1 Testing the results

Once the IMF, metallicity and observational parameters are assumed for a given galaxy, the positions of the observed stars in the CMD are used to construct the likelihood matrix $G_i(t)$, which is the only input given to the inversion method. In our Paper I we tested this method using synthetic CMDs produced from known $SFR(t)'s$, with which we could assess the accuracy of the result of the inversion procedure. In working with real data, we require the introduction of an independent method of comparing our final result to the starting CMD, in order to check that the answer our inversion procedure gives is a good answer. From our paper I we know that when the stars being used in the inversion procedure were indeed produced from the isochrones and metallicity used to construct the likelihood matrix, the inversion method gives accurate results. The introduction of an independent comparison between our answer and the data is hence a way of checking the accuracy of the input physics used in the inversion procedure, i.e. the IMF, metallicity and observational parameters.

The most common procedure of comparing a certain $SFR(t)$ with an observed CMD is to use the $SFR(t)$ to generate a synthetic CMD, and compare this to the observations using a statistical test to determine the degree of similarity between the two. For example, Aparicio et al. (1997) manage to recover simultaneously the distance, enrichment history and $SFR(t)$ of the local dwarf LGS 3 by constructing synthetic CMD's from a $SFR(t)$ taken parametrically as a series of contiguous bursts, and finding the amplitudes of each burst that give the maximum statistical similarity with the data, in terms of a counts in cells maximum likelihood. In that case, they solve for the amplitudes

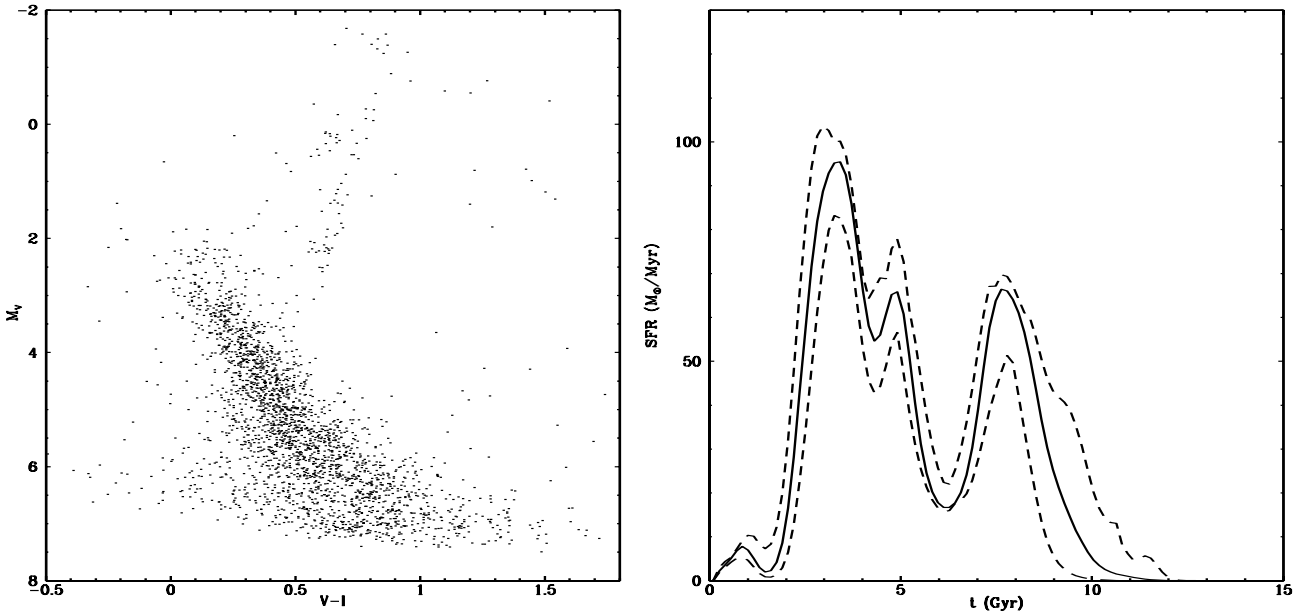

Figure 1.

Left: Observational HR diagram for Carina. **Right:** Inferred $SFR(t)$ for the central values of the observational parameters, solid line. The dashed curves represent the error envelope as defined by the quoted uncertainties in the foreground extinction and distance modulus.

of the bursts that give a total synthetic CMD most closely resembling the observational data set. Their synthetic CMD is a linear sum of the partial CMD's produced from a single realization for each burst. This has the advantage of allowing a large parameter space to be considered, as the synthetic CMD's are constructed trivially from a fixed single statistical realization of each burst. The disadvantage however is that one is not comparing the $SFR(t)$ with the data, but rather a particular realization of the $SFR(t)$ with the data. The distinction becomes arbitrary when large numbers of stars are found in all regions of the CMD, which is generally not the case. Following a Bayesian approach, we prefer to adopt the W statistic presented by Saha (1998), essentially

$$W = \prod_{i=1}^{B} \frac{(m_i + s_i)!}{m_i! s_i!}$$

where B is the number of cells into which the CMD is split, and m_i and s_i are the numbers of points two distributions being compared have in each cell. This asks for the probability that two distinct data sets are random realizations of the same underling distribution. In implementing this test we first produce a large number (~ 500) of random realizations of our best answer $SFR(t)$, and compute the W statistic between pairs in this sample of CMD's. This gives a distribution which is used to determine a range of values of W which are expected to arise in random realizations of the $SFR(t)$ being tested. Next the W statistic is computed between the observed data set, and a new large number of random realizations of $SFR(t)$, this gives a new distribution of W which can be objectively compared to the one arising from the model-model comparison to assess whether both data and modeled CMD's are compatible with a unique underling distribution. Both distributions of W were characterized in terms of a mean value and a 1σ amplitude. This final check of our answer is in fact the slowest part of the procedure, but necessary to obtain an independent check on the answer of our inversion method. In other terms, we are checking that our best inferred maximum-likelihood solution is also a good fit. The value of B used was ~ 6400.

4 THE GALAXIES

4.1 Carina

The first galaxy we study is the Carina dwarf, one of the first dSph's to be observed in terms of resolved stellar population, and the one for which the most studies inferring the $SFR(t)$ from the CMD have been published. This gives us the opportunity of comparing our results with previous studies. Our CMD diagram initially contained 2550 stars. After removing contamination, stars beyond the RGB and the lower degenerate region, we are left with 980 stars. The full observational CMD is shown in the left panel of Figure (1).

Using the numbers published in the recent review by Mateo (1998) we took as the central values of our observational parameters for Carina $[Fe/H] = -2.0 \pm 0.2$, $M_V = -9.3$, $E(B-V) = 0.04 \pm 0.02$ and $(m-M)_0 = 20.03 \pm 0.09$ (Smecker-Hane et al. 1994, Mighel 1997, Hurley-Keller et al. 1998 and Mateo et al. 1998). The metallicity fixes the isochrones and the integrated magnitude the normalization, we use the distance modulus and the reddening correction

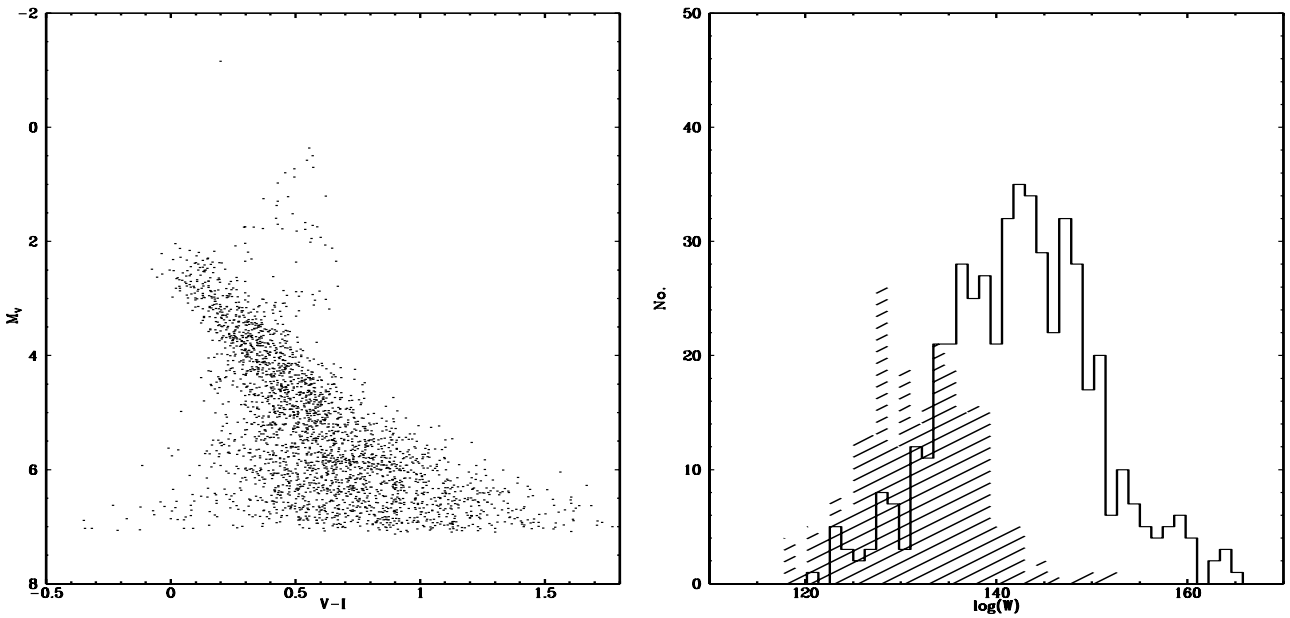

Figure 2.

Left: One synthetic HR diagram for Carina produced using the central inferred $SFR(t)$ of Figure (1). **Right:** Distribution of values of W arising from 500 model-model comparisons, unshaded histogram. This establishes the range of values of W which result from random realizations of the inferred $SFR(t)$. Also shown is the distribution of values of W arising from 250 data-model comparisons, showing the hypothesis that the data result from the same underlying function as the models to be acceptable at more than 1 sigma level.

to fix the observations in the CMD. At this point we apply our method to invert the observational CMD and recover the underlying $SFR(t)$, this is shown in the right panel of Figure (1) by the solid curve. The dotted curves represent the upper and lower envelopes to a series of alternative reconstructions of the $SFR(t)$ produced by changing the assumed values of the distance modulus and the reddening corrections, within their respective error ranges. The internal metallicity spread present in this galaxy is very low, as can be seen from the narrow RGB, and is quoted as < 0.1 dex in the review by Mateo (1998). In this way, our error margins for this galaxy due to metallicity uncertainties are not much larger than what is shown by the dotted lines, see Table(1).

In Figure (2) we illustrate the procedure of checking the inferred $SFR(t)$, the left panel gives one random realization of the central inferred $SFR(t)$, which is seen to resemble the data for Carina rather well. The right panel of Figure (2) shows the implementation of the W test. The solid histogram gives the distribution of values of W which arise from 500 model-model comparisons, and gives the variability arising from the different random realizations of the central $SFR(t)$, for the number of stars present in our observations. The dashed histogram gives the distribution of values of W which result from 250 data-model comparisons. Only < 32 % of the random realizations of our central $SFR(t)$ would give distributions of W (when compared against all other realizations) having a mean value further removed from that of the 500 model-model distribution than the data. In this sense, we can accept the hypothesis that both the data and our 500 random realizations of the central $SFR(t)$ for Carina come from the same underlying generating function at a 1 σ level. For the remaining galaxies we shall give only the results of the W test in terms of the mean and 1σ amplitude of the model-model and the data-model distributions.

Our result shows an interesting $SFR(t)$ for this galaxy, very little star formation at early times, until around 10 Gyr ago, when over a period of 3 Gyr an intermediate population was formed. The $SFR(t)$ then decreased markedly, before entering a more recent and extended period of star formation which ended 2 Gyr ago. The very low levels found throughout for the star formation rate of $50 - 100 M_{\odot}/Myr$ are representative of what we find in all our galaxies, and should provide clues as to the physical processes driving the star formation activity in these systems.

The existence of some RR Lyr stars in this galaxy (e.g. Saha et al. 1986, Mateo et al. 1995 or Kuhn et al. 1996) signal the presence of a very old population at some level, although recent estimates of the $SFR(t)$ in Carina coincide in that the amplitude of this old component is minor (Hurley-Keller & Mateo 1998), and appears to have blended completely into the MS of our CMD, or to be found preferentially in a region of the galaxy not sampled by our observations. One of the most general claims about the $SFR(t)$ of Carina has been the extreme "bursting" character of it (e.g. Smecker-Hane 1994, Hurley-Keller & Mateo 1998) we note however, that all these studies have assumed *a priori* an extremely discrete form for the $SFR(t)$ of this galaxy, and then solved for the best such function. In contrast, Mighell (1997) using a non-parametric approach, finds a much more continuous solution, basically consistent with what we obtain. The res-

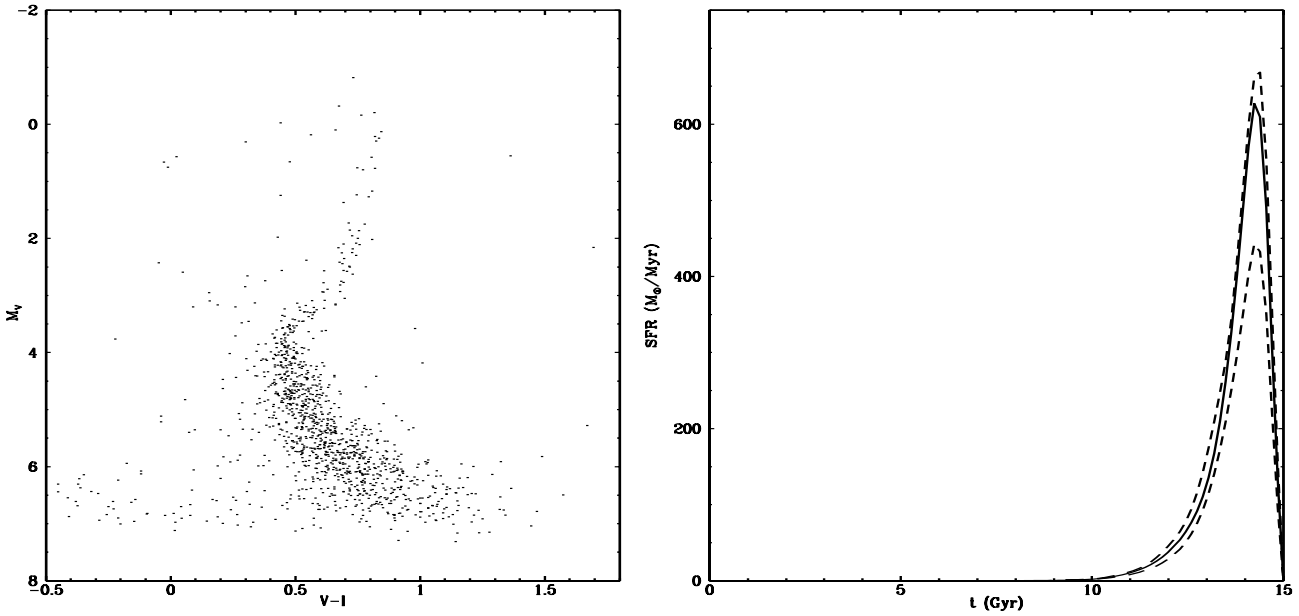

Figure 3.

Left: Observational HR diagram for Ursa Minor. **Right:** Inferred $SFR(t)$ for the central values of the observational parameters, solid line. The dashed curves represent the error envelope as defined by the quoted uncertainties in the foreground extinction and distance modulus.

olution of our method in the region of ages $2-8Gyr$ is sufficient to exclude the possibility of any total cessation of the star forming activity in this region lasting more than $0.5Gyr$, as was shown in our Paper I, where synthetic HR diagrams produced from bursting $SFR(t)'s$ were correctly inverted. We conclude that although the star formation history of this galaxy is clearly bimodal, it is not a series of discrete bursts lasting $\leq 1Gyr$. However, we can not exclude the possibility that sampling a much larger fraction of this galaxy could yield somewhat different results. Analyzing local variations of the $SFR(t)$ within these galaxies is an interesting project which will be treated in other papers, using data covering greater portions of the galaxies. As with all our galaxies, given the small number of stars available, the resolution of our solution is limited. Episodes of very short duration or low level, resulting in very few stars will be totally missed. We are recovering the $SFR(t)$ responsible for producing the greater fraction of the observed stars.

4.2 Ursa Minor

The case of Ursa Minor seems to be the simplest of the ones we study, and is actually the only one of our galaxies which agrees with the once common expectation of dSph systems being simply old and metal poor. Our observational CMD is shown in the left panel of Figure (3), and is made up of 1232 stars. After removing those stars incompatible with the phases included in our isochrones, together with the fraction beneath $M_V = 6$ we are left with 334 stars, which we used in the inversion procedure.

Using the values given in Mateo's (1998) review, we take $[Fe/H] = -2.2 \pm 0.1, M_V = -8.9, E(B-V) = 0.03 \pm 0.02$ and $(m-M)_0 = 19.11 \pm 0.1$ (Nemec et al. 1988 and Olszewski & Aaronson 1985) for this galaxy. The reported internal metallicity dispersion in this galaxy is also very low, at < 0.2 dex, which introduces little uncertainty in our results. Applying our method using the central values of the observational parameters we obtain the solid line shown in the right panel of Figure (3). Again, the dotted curves represent an envelope to a large number of reconstructions obtained by changing the observational parameters within their error ranges. Of this galaxy we can say that most of its stars are older than 12 Gyr. Given the observational errors present and the large age of the population of this galaxy, we can not draw any inferences on the time structure of the $SFR(t)$, as this is totally lost in the noise. The duration of the star forming episodes can only be concluded to have been $\leq 3Gyr$. Normalizing through the total luminosity of this galaxy we obtain rates of $> 400 M_\odot/Myr$. The result of applying the W test to this galaxy gives 47 ± 5 and 44 ± 4 for the model-model and model-data sets, respectively, showing our answer to be compatible with the data at better than a $1\,\sigma$ level. Olszewski & Aaronson (1985) used a ground based CMD and a simple isochrone fitting procedure to conclude the population of this galaxy is uniformly old, with the possibility of a 2Gyr spread.

4.3 LeoI

The observations we obtained for LeoI are shown in the CMD in the left panel of Figure(4). This contains 11334 stars, which was reduced to 8691 after exclusion of unsuitable stars (e.g. the red clump), as described for the previous two galaxies. The excluded region comprised stars with

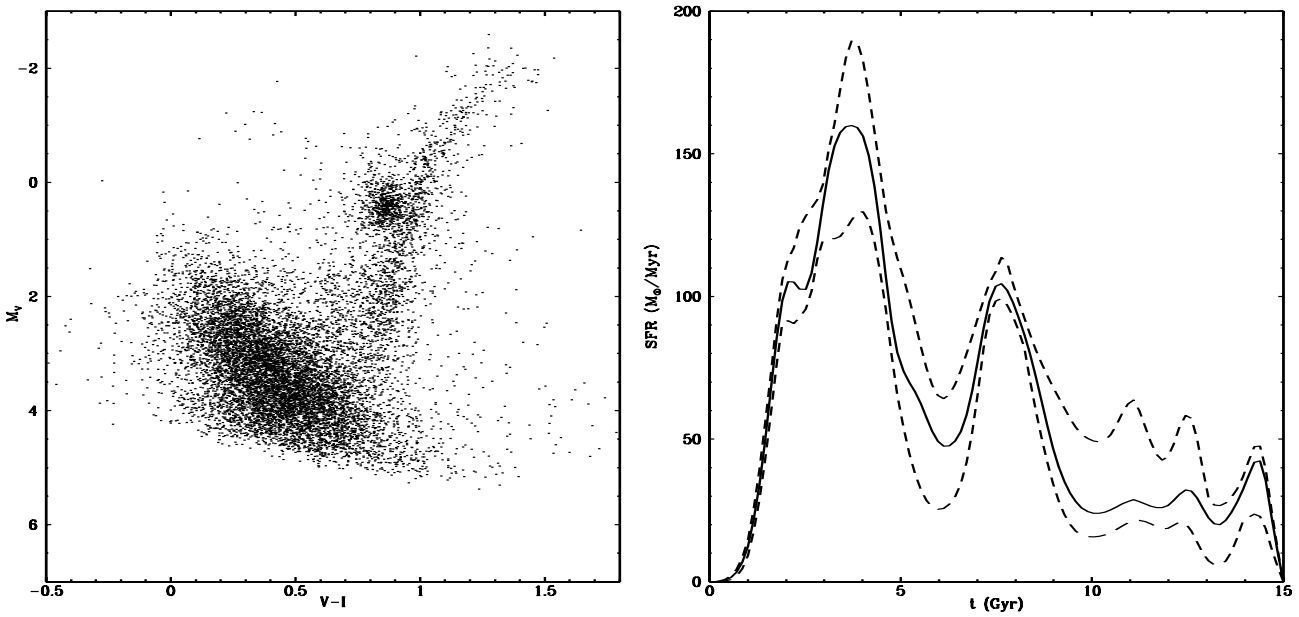

Figure 4.

Left: Observational HR diagram for Leo I. **Right:** Inferred $SFR(t)$ for the central values of the observational parameters, solid line. The dashed curves represent the error envelope as defined by the quoted uncertainties in the foreground extinction and distance modulus.

$M_V < 1$ and $B-V > 0.7$ and $B-V < 0.9$, though our results are highly insensitive to the details of these cut, as the RGB close to the red clump is an age degenerate region. The CMD of this galaxy reveals a young MS, but also a RGB extending down into the turn off region of a much older MS. The distribution of stars along the MS region is not uniform, and is actually encoding an interesting $SFR(t)$.

Taking for this galaxy the central values of those given by Mateo (1998), $[Fe/H] = -1.5 \pm 0.4, M_V = -11.9, E(B-V) = 0.01 \pm 0.01$ and $(m-M)_0 = 21.99 \pm 0.2$ (Reid & Mould 1991, Lee et al. 1993b and Demers et al. 1994), we invert the CMD of LeoI to obtain the $SFR(t)$ shown by the solid curve in the right panel of Figure (4). The dotted curves contain all other possible answers compatible with our method and the observational parameters taken with their errors.

The $SFR(t)$ of LeoI can be divided into three distinct phases, which join continuously with no evidence of a discrete bursting behaviour. The first of these phases lasted from $15 - 10Gyr$ ago, and proceeded at a rate of around $30 M_\odot/Myr$. The following two phases were extended peaks of star formation activity centered on ages of 8 and $4Gyr$, and having durations and maximum amplitudes of around 3 and $4Gyr$, at 100 and 150 $M_\odot/Myr$ respectively, as shown in Figure (4). Any total cessation of the star forming activity can be excluded for ages between 1 and 10 Gyr. As time resolution is lost beyond this age, the population beyond 10 Gyr could in principle be a single burst, and appear extended because of the observational errors.

The ground based study of Lee et al. (1993) reaching only the youngest turn off points, and subsequent analysis of this data set by Caputo et al. (1995) and Caputo et al. (1996) using isochrone matching techniques and luminosity function methods developed for single age globular clusters, revealed the presence of stars of ages 1-3 Gyr. Using more recent HST data and comparing to modeled CMDs Gallart et al. (1998) describe the star formation history of LeoI as coming mostly from an episode lasting from 6-2 Gyr ago, with the addition of an older component of duration 2-3 Gyr, in good agreement with our inferred $SFR(t)$ for this galaxy. The population box of this galaxy given by Mateo (1998) is consistent with our results.

In this case, the W test gives results showing that our inferred $SFR(t)$ is incompatible with the data at a two σ level. As our inversion method has been extensively tested using synthetic CMD's, this result shows the data to be in conflict with our input assumptions. This is perhaps not surprising as this system has a much larger internal metallicity spread (0.3 ± 0.1) than the two reviewed previously, which together with the errors in the metallicity determination allow for quite a large (~ 1) internal spread. We have thus solved for the best fitting single metallicity solution, and discovered that internal metallicity dispersions are important. This metallicity spread introduces a time uncertainty going from 1-3 Gyr, for ages going from 1-13 Gyr. Solving simultaneously for the enrichment and star formation histories is a problem we shall treat later, as an extension of the variational calculus approach. A further possible source of the disagreement found between the synthetic CMD reproductions of our recovered $SFR(t)$ and the data is the difficulty of modeling precisely the error structure present in real data, as pointed out by Aparicio & Gallart (1995). Although the inversion method itself is highly robust to the details of the assumed error structure, the very careful comparison of the W test would pick up any discrepancy be-

tween the assumed error structure used in generating the synthetic CMD's, and that actually present in the data. Finally, the presently available isochrones do not take into account the relative overabundance of α elements at low metallicities, which at some level introduces a slight mismatch between the observed stars and the assumed modeling. Unfortunately, we can not distinguish between these possibilities easily.

4.4 LeoII

For this galaxy we obtained 7625 stars, of which we used 4492 after removing from the analysis the red clump (stars with both $M_V < 1$ and $B - V < 0.9$), the lower regions and some blue stragglers blue wards of $V - I = 0.2$, which do not correspond to any of the evolutionary phases included in our isochrones. The full observational CMD is shown in the left panel of Figure (5). For the central values of the observational parameters of this galaxy as summarized by Mateo (1998) of $[Fe/H] = -1.9 \pm 0.1, M_V = -8.9, E(B-V) = 0.02 \pm 0.01$ and $(m-M)_0 = 21.63 \pm 0.09$ (Mighel & Rich 1996, Demers & Irwin 1993 and Lee 1995) we obtain a divergent solution, indicating that the isochrones used do not correspond to the stars being analyzed. Changing the metallicity to $[Fe/H] = -1.75$, just marginally outside the errors reported by Mateo (1998), gives a stable convergence of the method and a significant result. The recent study by Mighell and Rich (1996) determined a metallicity of $[Fe/H] = -1.6 \pm 0.25$ for this galaxy, consistent with what was used here. Our inferred $SFR(t)$ is shown by the solid curve in the right panel of Figure (5). Again, the dotted curves represent an envelope to all alternative reconstructions obtained by varying the observational parameters within their errors. As with LeoI, this galaxy shows a large internal metallicity spread, which is probably what the very sensitive W test detects, also giving an incompatible result between the model-model and data-model comparisons at more than a two σ level. The discussion of this point given for the previous galaxy applies also to LeoII, metallicity spreads will have to be considered for a more accurate rendering of the star formation history of this galaxy.

In this case, we see a gradually rising SFR from 12 Gyr to a peak of 160 $M_\odot/Myr$ at 8 Gyr, followed by a somewhat more abrupt descent, with star formation activity ending by around 6 Gyr ago, as shown by Figure (5). This result would be affected by the internal metallicity spread of 0.3 dex of LeoII (Mateo 1998), producing a broadening of around 1-3 Gyr, see Table (1). Comparing with the study of Mighell and Rich (1996), who analyze an HST CMD of LeoII by fitting a "fiducial sequence" to the CMD and then comparing it to theoretical isochrones to solve for the age of the galaxy treated as a single parameter, we find no inconsistencies. They obtain an age of 9 ± 1 Gyr for LeoII, with an age spread of around 4 Gyr, which is compatible with our results. They also report some degree of star formation at ages $> 10Gyr$, of which we see no evidence. This discrepancy is probably the result of the different methods used in the analysis. Given the high age resolution of our method, it is not only the median age and a representative value for the spread that we obtain, also the shape of the burst is recovered, ruling out for example a rectangular burst for this galaxy. Not just the age and duration of star formation episodes in these galaxies, but also the time structure of them can now be reliably inferred, and used in aiding theoretical interpretations of the origin of these systems.

4.5 Draco

For this last galaxy our observational CMD contains 3091 stars, most of which are located in the lower, age-degenerate region of the diagram, and were thus excluded from the analysis, leaving 1210 stars after removing also the horizontal branch and blue stragglers (stars with both $M_V < 0$ and $B - V < 0.7$). Our full observational CMD for Draco is shown in the left panel of Figure (6). Mateo (1998) summarizes the metallicity and observational properties as $[Fe/H] = -2.0 \pm 0.15, M_V = -8.8, E(B-V) = 0.03 \pm 0.01$ and $(m-M)_0 = 19.58 \pm 0.15$ (Carney & Seitzer 1986, Lehnert et al. 1992, Nemec 1985 and Grillmair et al. 1998). Using the central values we produced our observational CMD and inverted it to obtain the $SFR(t)$ plotted as the solid curve in the right panel of Figure (6). The dotted curves contain all variations obtained by shifting our observations within the error ranges of the values given by Mateo (1998) for $E(V-I)$ and $(m-M)_V$.

Our result for Draco is very similar to what we obtained for LeoII, only shifted by 2 Gyr towards younger ages, giving a median age of around 7 Gyr. The time structure of the $SFR(t)$ also differs slightly from that of LeoII in that the peak is broader in Draco, having a plateau lasting around 2 Gyr, rather than a narrow maximum. The presence of a low level old component extending beyond 10 Gyr is also inferred, although the precise time structure in this region is not well restricted by the method. The values given by the normalization through the total luminosity are in the range of our other galaxies, with the maximum rate being of around 110 $M_\odot/Myr$. Using Saha's W test in this case gives 208 ± 9 for the model-model comparison, and 201 ± 8 for the data-model comparison, which gives us confidence in our results, as it shows our $SFR(t)$ is compatible with the data at better than a 1 σ level.

Comparing this result with the recent study of Grillmair et al. (1998) we find the two results to be only marginally consistent, as they report an age of 10-12 Gyr (for the IMF we assumed) for the bulk of the stellar population of Draco $\pm 2.5Gyr$, which they identify as essentially a single age event. We note several differences between their approach and ours, any of which on its own could bring the two results into closer agreement. They use HST data to construct their observational CMD, which is very similar to the one we obtain, no differences are evident at this level. Their analysis however differs markedly. They fit a fiducial sequence to the CMD diagram assumed to be representative of the bulk of the population, adjusting the MS and lower RGB regions through an inclusion envelope criterion, and the bright RGB by eye. This fiducial sequence is then compared to theoretical isochrones (VandenBerg & Bell 1985) through a maximum likelihood analysis designed to find the age of the system, treated as a one parameter problem. We note that comparing any fiducial sequence to theoretical isochrones will only be a meaningful statistical procedure in cases where the underlying $SFR(t)$ is indeed

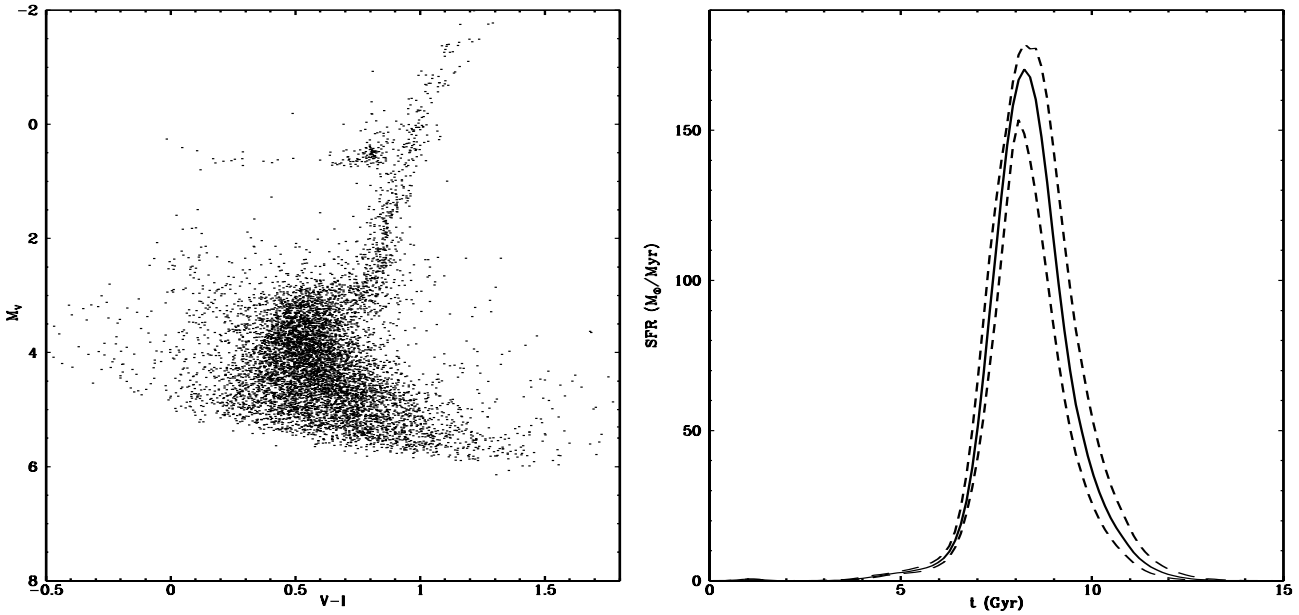

Figure 5.

Left: Observational HR diagram for Leo II. **Right:** Inferred $SFR(t)$ for the central values of the observational parameters, solid line. The dashed curves represent the error envelope as defined by the quoted uncertainties in the foreground extinction and distance modulus.

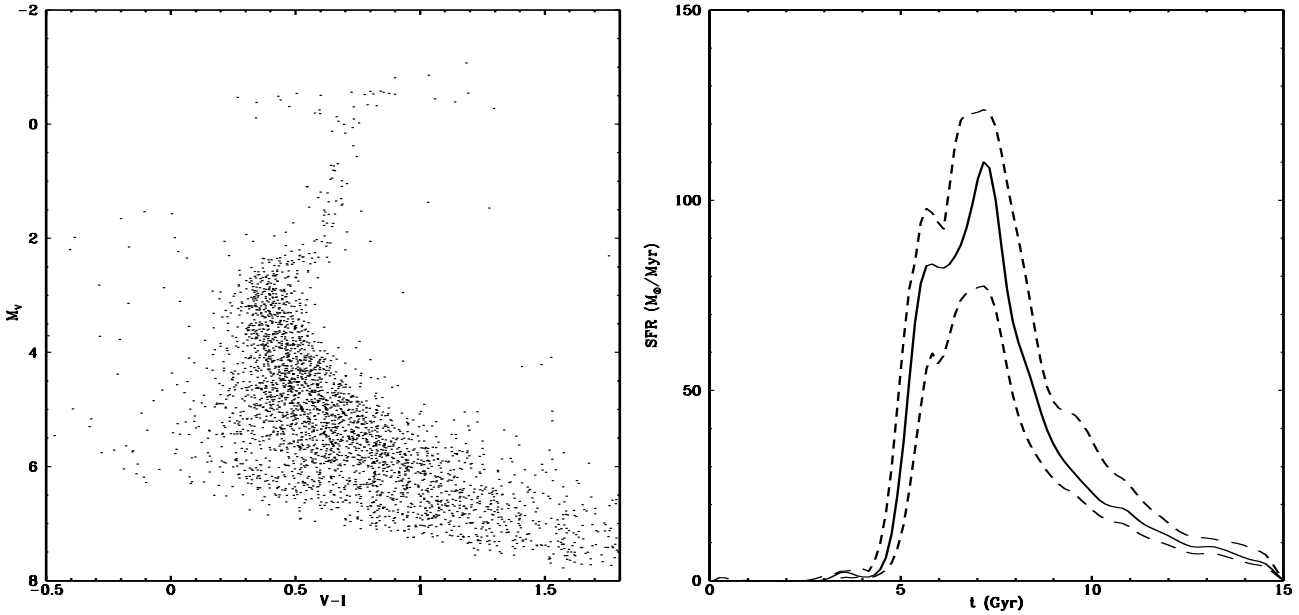

Figure 6.

Left: Observational HR diagram for Draco. **Right:** Inferred $SFR(t)$ for the central values of the observational parameters, solid line. The dashed curves represent the error envelope as defined by the quoted uncertainties in the foreground extinction and distance modulus.

a single epoch burst, e.g. in the case of a globular cluster. Further, defining any such sequence so that it is a valid statistical representation of the underlying $SFR(t)$ is a problem that has not been treated yet. Grillmair et al. (1998) also noted their isochrones showed systematic inconsistencies when compared to the stars they were dating, which also casts some doubt on their results, as they remarked. They also had the difficulty of requiring multiple conversions between their observational bands and those available from theoretical stellar models.

Our results for this galaxy are weakened by the assumption of a single metallicity for the entire population. Although this can not be rigorously correct, it essentially holds for the previous four galaxies, which show small internal metallicity spreads. Draco however, has an internal spread of 0.5 dex (Mateo 1998), which could alter our results for this galaxy at the level of 1-3 Gyr. Another possible explanation to the difference between our results and those of Grillmair et al. (1998) is that we used the Padova isochrones (Fagotto et al. 1994, Girardi et al. 1996) rather than those of VandenBerg & Bell (1985). Finally, we note that Carney & Seitzer (1986) sampled a much larger region of Draco using ground based CCD data, and detected multiple turnoffs in this galaxy, corresponding to ages between 8 and 15 Gyr.

5 SUMMARY

We have used a homogeneous set of observational colour magnitude data to study the star formation histories of a sample of 5 dSph galaxies, through a non-parametric variational calculus maximum likelihood method. We then performed a detailed statistical analysis to check the accuracy of our results for each galaxy, obtaining good results for three of our galaxies (Carina, Ursa Minor and Draco), and evidence of a systematic difference between our data and results for LeoI and LeoII, probably due to internal metallicity spreads. We can now compare the results we obtained for the different galaxies, with the added consideration of a possible extra 1-3 Gyr error margin in the results for LeoI and LeoII.

Ursa Minor appears to be the only essentially "Population II" system, being characterized by a uniformly old star formation history. LeoII and Draco are systems which show similar star formation histories, being basically characterized by a single major episode. This lasted in both cases around 4 Gyr centered at 8 Gyr, although Draco shows a low level extension into much older ages. LeoI shows the most complex $SFR(t)$, having a small old component of age > 10 Gyr, and two later episodes centered at 8 and 3.5 Gyr, although the star formation activity did not stop altogether between them. It is interesting that the second episode in LeoI coincides in age with the period of star formation in Draco and LeoII. Finally, star formation in Carina highly resembles that in LeoI in the relative amplitude, duration and locations of the two main components.

Since we used the total luminosities of these galaxies to normalize the inferred $SFR(t)$ in physical units, we can derive other quantities of interest, for example the supernova rates as a function of time. The SN type II rates are obtained by scaling the total $SFR(t)$ by a factor given by the fraction of stars more massive than $8M_{\odot}$, which for our assumed IMF translates $100M_{\odot}/Myr \approx 1SNII/2Myr$. The only galaxy showing rates greater than $150M_{\odot}/My$ is Ursa Minor, and it is also the only one with a $SFR(t)$ consistent with a single epoch burst. The other four systems, showing extended $SFR(t)'s$, have rates of always less than $150M_{\odot}/Myr$. This last fact might indicate the presence of a threshold in these systems, above which energy input from massive stars into the gas component is sufficient to totally disrupt the galaxies interstellar medium and end star formation. No characteristic timescales of ~ 1 Gyr are evident from the recovered $SFR(t)'s$ of these galaxies, with the possible exception of Ursa Minor, suggesting that SN type I are not determinant in driving the star formation processes in these systems.

Figure (7) presents the luminosity weighted sum of the $SFR(t)$ for all the galaxies we analyzed. This shows the star formation activity in the set of these low metallicity dSph's to have ended by around 2 Gyr ago, and having been relatively steady during the period 3-9 Gyr. For older ages we see the average $SFR(t)$ to be essentially dominated by the old age Ursa Minor galaxy. Our results as summarized by Figure (7) support the calculations presented by Unavane et al. (1996) in that the average metal-poor dSph star is of intermediate age, and not as old as a "Population II" halo star. A more complete sample would include the Sagittarius dwarf, with a mean age of $\approx 10Gyr$, as well as the much larger Magellanic clouds, having ages of $< 3Gyr$. It seems reasonable to suppose the total star formation history for the satellites of the Milky Way to show no preferred epoch of star formation, as suggested by Tolstoy (1998).

From these comparisons it is clear that the dSph galaxies of the Milky Way do not form a simple system, and straight forward correlations between $SFR(t)$ and other present day parameters such as instantaneous galactocentric distance or metallicity are not evident, and perhaps not even meaningful. A physical understanding of these systems will probably have to consider the complex interactions of these systems with the halo of the Galaxy (tidal forces, evolving gaseous component, orbital structure etc). It could well be the case that the present day sample of survivors actually experienced very distinct origins and evolutionary histories (as direct studies of their $SFR(t)$ appear to indicate) with little in common other than having been shaped under the dominating influence of the Milky Way. A ram pressure stripped dwarf irregular and a more recently tidally torn fragment of the Magellanic clouds could both end up as dSph systems today.

Much more information is needed on these systems before their full potential as tracers of the build up and evolution of the Milky Way can be realized, once their individual evolutionary histories are better understood. Studies aimed at recovering the full orbital structure of these galaxies, through proper motion measurements and potential theory reconstructions will yield crucial independent information on the evolution and formation of these systems. A more complete sampling than the one we have conducted here is needed to visualize local dSph's fully. Any advance in the modeling of advanced stellar phases will also improve the use of CMD as tools in galactic evolution studies, as it would in principle eliminate the need to remove parts of the CMD from consideration.

Our present sample includes the 5 dSph galaxies having the lowest internal metallicity spreads, and therefore the

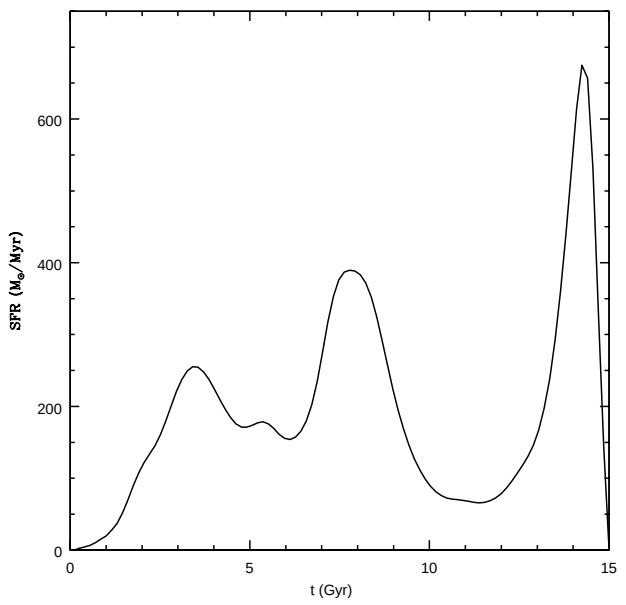

Figure 7. Sum of the $SFR(t)'s$ of the five galaxies we studied

ones for which our present method applies best. Obtaining a larger sample and analyzing it through a fully consistent and non parametric statistical method, will require the simultaneous recovering of the enrichment history and the $SFR(t)$. Development of such a method will be the subject of a future work. We emphasize the need of a homogeneous sample at all levels of the analysis, together with a fully consistent statistical inversion method which does not assume any *a priori* structure for the $SFR(t)$ one is solving for, in comparative studies of star formation histories.

Acknowledgments

The work of X. Hernandez was partly supported by a DGAPA-UNAM grant.

REFERENCES

Aparicio A., Bertelli G., Chiosi C., Garcia-Pelayo J.M., 1990, A&A 240, 262
Aparicio A., Gallart C., 1995, AJ, 110, 2105
Aparicio A., Gallart C., Bertelli G., 1997, AJ, 114, 680
Caputo F., Castellani V., Degl' Innocenti S., 1995, A&A, 304, 365
Caputo F., Castellani V., Degl' Innocenti S., 1996, A&A, 309, 413
Chiosi C., Bertelli G., Meylan G., Ortolani S., 1989, A&A, 219, 167
Carney B.W., Seitzer P., 1986, AJ, 92, 23
Demers S., Irwin M.J., 1993, MNRAS, 261, 657
Demers S., Irwin M.J., Gambu I., 1994, MNRAS, 266, 7
Elson R.A.W., Santiago B.X., Gilmore G.F., 1996, NewAst, 1, 1
Fagotto F., Bressan A., Bertelli G., Chiosi C., 1994, A&AS, 104,365
Gallart C., Freedman W., Aparicio A., Bertelli G., Chiosi C., 1998, AAS, 192, 177

Table A1. The dwarf spheroidal galaxy data used. The galaxy name, the date of observation, the HST archive image numbers and the filters used are given

Galaxy Name	Date of Observation	Image Filenames	Filters Used 'V'-filter	'I'-filter
Leo II	15 May 1994	u28v0101t-kt	F555W	F814W
Leo I	5 Mar 1994	u27ko101t-8t	F555W	F814W
Draco	9 Jun 1995	u2oco101t-6t	F606W	F814W
Carina	3 Jan 1995	u21b0101t-6t	F555W	F814W
Ursa Minor	4 Jul 1995	u2pb0101t-6t	F555W	F814W

Gerhard O.E., Spergel D.N., 1992, ApJ, 389, L9
Girardi L., Bressan A., Chiosi C., Bertelli G., Nasi E., 1996, A&AS 117, 113
Grillmair C.J., Mould J.R., et al., 1998, AJ, 115, 144
Hernandez X., Valls-Gabaud D.,Gilmore G., 1999, MNRAS 304, 705 (paper I)
Holtzman J.A., et al. 1995, PASP, 107, 1065
Hurley-Keller D., Mateo M., Nemec J., 1998, AJ, in press.
Kroupa P., Tout C.A., Gilmore G., 1993, MNRAS, 262, 545
Kuhn J.R., Smith H.A., Hawley S.L., 1996, ApJ, 469, L93
Lee M.G., 1995, AJ, 110, 1155
Lee M.G., Freedman W., Mateo M., Thompson I., Roth M., Ruiz M., 1993, AJ, 106, 1420
Lee M.G., Freedman W., Madore B.F., 1993b, AJ, 106, 964
Lehnert M.D., Bell R.A., Hesser J.E., Oke J.B., 1992, ApJ, 395, 466
Lin D.N.C., Faber S.M., 1983, ApJ, 266, 21
Mateo M., 1998, ARA&A, 36, 435
Mateo M., Fischer P., Krzeminiski W., 1995, AJ 110, 2166
Mateo M., Hurley-Keller., D.A., Nemec J., 1998, AJ, 115, 1856
Mighell K.J., Butcher H.R., 1992, A&A, 255, 26
Mighell K.J., Rich R.M., 1996, AJ, 111, 777
Mighell K.J., 1997, AJ, 114, 1458
Mould J.R., Han M., Stetson P.B., 1997, ApJ, 483, L41
Nemec J.M., 1985, AJ, 90, 204
Nemec J.M., Wehlau A., Mendez de Oliveira C., 1998, AJ, 96, 528
Olszewski E. W., Aaronson M., 1985, AJ, 90, 2221
Reid N., Mould J., 1991, AJ, 101, 1299
Saha P., 1998, AJ, 115, 1206
Saha A., Monet D.G., Seitzer P., 1986, AJ, 92, 302
Smecker-Hane T.A., Stetson P.B., Hesser J.E., Lehnert M.D., 1994 AJ, 108, 507
Tolstoy E., 1998, preprint, astro-ph/9807154
Tolstoy E., Saha A., 1996, ApJ, 462, 672
Unavane M., Wyse R.F.G., Gilmore G., 1996, MNRAS, 278, 727
VandenBerg D.A., Bell R.A., 1985, ApJS, 58, 561
Williams, R.E., et al. 1996, AJ, 112, 1335

APPENDIX A1: THE IMAGES

The images were recovered from the HST data archive. The image numbers, filters and observation dates are given in table A1. Table A2 gives the A-to-D gains, exposure times, and numbers of images for the dSph fields.

Table A2. The A-to-D gains, exposure times, and numbers of images for the dSph fields.

Galaxy Name	A-to-D gain	Total exposure (secs) 'V'-filter	'I'-filter
Leo II	7.0	4800	4800
Leo I	7.0	5700	4800
Draco	7.0	2000	2400
Carina	7.0	2200	2200
Ursa Minor	7.0	2100	2300

A1.1 Retrieving the data and image preparation

For each of the five dSph's, there were a number, n, of images taken, in both a long band (F814W, corresponding closely to Johnson's I), and a short band (F555W or F606W, corresponding to Johnson's V).

For each dSph, there are a set of long exposure 'V' and 'I' data files. Each data file contains the output from 4 detectors – the planetary camera (PC), and the three Wide Field cameras (WF2, WF3 and WF4). Each of these detector images is 800×800 pixels in size, of which typically 730×730 are usable.

Data treatment was carried out in the IRAF environment. Image combination was carried out using the STSDAS package, and photometry using the DAOPHOT package.

In order to remove the severe cosmic ray effects in each image, the n images were combined by taking the mean value for each pixel position, after the rejection of values either too high or too low with respect to local variations. The task used here was 'crrej' in the STSDAS package. Each image was also cropped to a 730×730 image by rejecting the first 60 rows/columns and the last 10.

In the following analyses, only the data from the three WF cameras were used. The pixel scale in these WF images is 0.10" per pixel.

A1.2 Source extraction

Sources were extracted to 2σ above the mean background. Point spread function (PSF) fitting photometry was carried out by selecting isolated stars to define a PSF. Sources with a fit at $\chi^2 > 1.5$ were rejected, and the magnitudes used were aperture magnitudes with a radius of 2 pixels. (0.20").

A1.3 Galactic contamination

At faint magnitudes in optical wavebands, external galaxies can constitute a major contaminant in number counts. Williams et al. (1996), based on HDF (Hubble Deep Field) galaxy counts find $\sim 2\times10^5$ galaxies per square degree brighter than V=26. For the area of the three WF detectors, this corresponds to, on average, 250 contaminating galaxies in the field of view. Compared with the many thousands of stars in the images, this contamination is small.

Nevertheless, the high resolution of the HST allows the separation of galaxies from stars more reliably than for ground based work, where image resolution is necessarily lower and the distinguishing stars from galaxies is less straightforward.

The cut in χ^2 which we use eliminates the majority of galaxies (and remaining cosmic ray events) because these will in general be fitted poorly by the PSF.

A1.4 Magnitude corrections

A1.4.1 Aperture Corrections

An aperture correction to render these magnitudes equivalent to those which would be obtained by use of a 0.5" radius aperture (see Holtzman et al. 1995) was found by selecting bright, unsaturated stars, in each of the 'V' and 'I' bands, and for each detector and each dSph separately. The mean differences between the magnitude using a 5.02 pixel diameter aperture (0.5" radius) and a 2 pixel diameter aperture were used to correct all magnitudes.

A1.4.2 A to D gain correction

All the observations for the dSph's considered here were taken through bay 4 (see Holtzman et al. 1995), which means that the Analogue-to-Digital gain is only 7.0, rather than the standard value of 14.0. Due to some unshared electronics, this necessitates a different correction for each of the WF fields, as indicated below:

Wide Field	Δm
2	0.754
3	0.756
4	0.728

A1.4.3 Geometric correction

The WF cameras have geometric distortions which arise mainly from elements in the optical path. As a consequence, the effective pixel areas, in square angular measure, vary systematically across each WF detector. We make a parameterization of the data from the figures of Holtzman et al. (1995), and apply that as a correction. The correction is well represented by a quadratic function of distance from the centre of the detector, and never exceeds 0.04 magnitudes at the edge of the detectors.

We use $\Delta m = -1.897\times10^{-5}\ r - 1.208\times10^{-7}\ r^2$ where r is the distance in pixels from the position (400,400) on the detector.

A1.4.4 Charge Transfer efficiency correction

The readout of the CCD detectors requires the transfer of charge through successive rows of the detector. As a consequence, the signal from the last rows to be read are diminished because of the loss of charge during transfers. The correction is a maximum of 0.04 magnitudes at the final row.

We use $\Delta m = -0.04(y/800)$ where y is the row number.

Table A3. The synthetic transformations from F555W and F606W to V, and from F814W to I, taken from Holtzman et al. (1995)

Filter	Constraint	Output Band	a_0	a_1	a_2
F555W	–	V	21.729	−0.051	0.009
F606W	(V−I)<1.0	V	22.093	0.254	0.012
F606W	(V−I)>1.0	V	22.883	−0.247	0.065
F814W	(V−I)<1.0	I	20.838	−0.012	−0.006
F814W	(V−I)>1.0	I	20.920	0.028	−0.124

A1.4.5 Corrections for Leo I

WFPC2 data taken before 23rd April 1994 was taken at a detector temperature of −76°C rather than −88°C. The change reduced CTE effects, and IR zeropoint problems. The Leo I observations were made before this change, and we use a linear ramp of size 0.12 magnitudes to correct for the CTE effects as recommended by Holtzman et al. (1995), and additionally, an additive offset of 0.05 magnitudes in I to correct for the higher zero point.

A1.5 Conversion to standard V and I

Reddening must be taken into account before corrections are made to V and I. We use the published values of reddening, which are fairly small for all these galaxies ($E(B-V) < 0.08$), to make corrections to the magnitudes before applying the transformations given below.

We use the extinction values tabulated by Holtzman et al. (1995) for the filter F555W and F814W, and an estimate based on these for the F606W filter:

$A_{F555W} = 3.026E(B-V)$

$A_{F814W} = 1.825E(B-V)$

$A_{F606W} = 2.75E(B-V)$ (estimate)

We subsequently apply synthetic transformations given by Holtzman et al. (1995), of the form

$$\text{Output Band} = m_{raw} + a_0 + a_1(\text{V}-\text{I}) + a_2(\text{V}-\text{I})^2$$

where the coefficients are given in table A3.

m_{raw} is the output aperture magnitude using an aperture of 2 pixels radius, corrected as indicated above to an aperture of radius 0.5".

The above formulae were iterated until no further significant change in V or I occurred.

Finally, the reddenings which had been removed are restored using:

$A_V = 3.10E(B-V)$

and

$A_I = 1.83E(B-V)$

The reddenings used are refined iteratively after the fitting of isochrones to the MS region. Note, however, that because the reddenings are small, and the reddenings are restored to the data afterwards, even if the initial guess for the reddening is wrong by a substantial amount, very little effect is seen in the final photometry. (e.g. a change of the reddening by 0.1^m changes photometry by less than 0.005^m.)

A1.6 Systematics

As Holtzman et al. (1995) point out, there remain some aspects of the photometric calibration of WFPC2 which are uncertain. For example, Holtzman et al.(1995) note discrepancies of ~ 0.05 magnitudes between long and short exposures, which are not understood. Several more minor systematic and random effects at the level of a few percent (corresponding to a few hundredths of a magnitude) are not well understood. Furthermore, the conversion that has been made here to standard V and I colours, introduces more minor uncertainties. It must be noted that the systematic effects in zeropoints may be as large as 0.1 magnitudes. Any such uncertainties appear as an offset primarily in adopted distance modulus, and would affect most CMDs in the same way. Differentially, any effects should be minimal.